Pharmaceutical Sciences and Drug Design
ISSN: 3062-4428
2023, Volume 3, Page No: 157-175

Available online at: www.galaxypub.co/page/journals

Galaxy Publication

Galaxy Publication

Mechanistic Insights into Radix Paeoniae Rubra and Radix Angelicae Sinensis Granules for Diabetes-Induced Erectile Dysfunction Using Network Pharmacology and In Vivo Studies

Charlotte Reed[1]*, Wyatt Turner[1], Penelope Gray[1]

[1]Department of Biotechnology, Faculty of Medicine, McGill University, Montreal, Canada.

***E-mail** ✉ charlotte.reed.ca@outlook.com

Received: 07 August 2023; **Revised:** 21 October 2023; **Accepted:** 24 October 2023

ABSTRACT

Diabetes mellitus-induced erectile dysfunction (DMED) remains a challenging condition without effective targeted therapies. This study aimed to explore the potential mechanisms and molecular targets of Radix Paeoniae Rubra and Radix Angelicae Sinensis Granules (RAG) in DMED using a combination of network pharmacology and experimental validation. Active compounds of RAG and their predicted targets were retrieved from the Traditional Chinese Medicine Systems Pharmacology Database (TCMSP). DMED-related genes were collected from GeneCards, OMIM, and PharmGKB. Shared targets were identified and used to construct protein-protein interaction networks. A drug–ingredient–disease–target network was established using Cytoscape, and functional enrichment analyses (GO and KEGG) were performed via OmicShare. Molecular docking was carried out with Molecular Operating Environment (MOE) software to assess compound–target interactions. Finally, the therapeutic effects of RAG were evaluated in DMED rat models.

Twenty bioactive constituents and 25 overlapping targets were identified, implicating pathways associated with vasodilation, apoptosis, protein secretion, and hypoxia. Enriched pathways included HIF-1, MAPK, cAMP, and Ras signaling. Six hub genes—INS, CAT, BDNF, CASP3, CRP, and HMOX1—were predicted as primary targets of RAG. Docking studies showed strong binding affinities of oleic acid, catechin, and butylated hydroxytoluene to these targets. In vivo, RAG administration improved penile hemodynamics, enhanced nitric oxide production, ameliorated histopathological changes, upregulated eNOS, iNOS, and HMOX1, and downregulated HIF-1 expression. The findings suggest that RAG may exert protective effects against DMED through modulation of the HIF-1α/HMOX1 pathway. This study provides mechanistic insights supporting the potential use of RAG as a therapeutic strategy for DMED.

Keywords: Radix Paeoniae Rubra, Diabetes mellitus, Radix Angelicae Sinensis, Erectile dysfunction, Hub genes, Network pharmacology, HIF-1 signaling

How to Cite This Article: Reed C, Turner W, Gray P. Mechanistic Insights into Radix Paeoniae Rubra and Radix Angelicae Sinensis Granules for Diabetes-Induced Erectile Dysfunction Using Network Pharmacology and In Vivo Studies. Pharm Sci Drug Des. 2023;3:157-75. https://doi.org/10.51847/iWtQWj6RsG

Introduction

Erectile dysfunction (ED) is defined as the persistent inability to achieve or maintain an erection sufficient for satisfactory sexual performance for at least six months. It is among the most prevalent sexual disorders in andrology [1], significantly affecting patients' quality of life and family relationships. Diabetes mellitus (DM) is a common cause of ED, and patients with DM exhibit a 3.5-fold higher risk of developing ED compared with non-diabetic individuals [2]. Moreover, ED occurs 10–15 years earlier and tends to be more severe in patients with DM [3], with a reported global prevalence ranging from 20% to 75% [4, 5]. The pathogenesis of DM-induced ED (DMED) is multifactorial, involving vascular endothelial dysfunction, atrophy of cavernous smooth muscle, neuropathy, and fibrosis, with endothelial dysfunction considered the primary pathological basis [6]. Although phosphodiesterase type 5 (PDE5) inhibitors are first-line treatments for ED, many DMED patients fail to achieve

satisfactory outcomes, as these drugs do not address underlying diabetic pathology [6]. Thus, identifying new therapeutic strategies and elucidating their molecular mechanisms is crucial for managing DMED.

Endothelial dysfunction in DMED is associated with impaired nitric oxide (NO) synthesis and reduced bioavailability [7]. Under normal conditions, NO is produced by three nitric oxide synthase (NOS) isoforms: endothelial NOS (eNOS), neuronal NOS (nNOS), and inducible NOS (iNOS). Impaired endothelial function, particularly decreased eNOS activity and expression, is a key factor in the limited efficacy of PDE5 inhibitors in DMED patients [8].

Hyperglycemia and advanced glycation end products (AGEs) are known to activate hypoxia-inducible factor 1-alpha (HIF-1α) [9], a critical mediator in hypoxic and ischemic conditions. HIF-1α regulates intracellular oxygen balance and glucose metabolism through downstream effectors, especially in vascular endothelial and smooth muscle cells [10, 11]. In diabetic rat models, prolonged HIF-1α activation and AGE accumulation reduce NOS production, decrease NO bioavailability, promote fibrosis of cavernous tissue, and induce smooth muscle apoptosis, collectively contributing to ED [12, 13]. Therefore, strategies that increase NOS activity, enhance NO availability, and suppress HIF-1α may represent effective therapeutic approaches for DMED.

Medicinal plants have long been used to manage diabetes. For example, *Cassia glauca* is widely employed in traditional Indian medicine as a natural hypoglycemic agent by improving insulin sensitivity and lowering blood glucose [14]. Similarly, Radix Paeoniae Rubra (RPR) and Radix Angelicae Sinensis (RAS) are traditional Chinese medicinal herbs historically used to treat blood disorders, diabetes, and related conditions. RPR is believed to clear heat, cool the blood, promote circulation, and remove stasis [15], and pharmacological studies have confirmed its anti-thrombosis, anti-platelet aggregation, hypoglycemic, lipid-lowering, and anti-atherosclerotic effects [15, 16]. RAS is known to replenish blood, regulate menstruation, and relieve pain; it also exhibits vasodilatory, hemorheological, and anti-atherosclerotic properties [17, 18]. Accordingly, RPR and RAS are commonly combined in traditional practice to improve blood circulation, alleviate stasis, and treat diabetic complications [19, 20]. However, the multiple components, targets, and pathways of this combination have limited comprehensive mechanistic studies. Systematic evaluation is therefore essential to better understand its therapeutic potential in DMED.

Network pharmacology offers a systematic framework for investigating drug-disease interactions by integrating biological data and network analyses [21]. Given the multi-component and multi-target characteristics of traditional Chinese medicine, network pharmacology is particularly suitable for elucidating the mechanisms of herbal compounds [22]. In this study, we employed network pharmacology to identify the active compounds and potential targets of RPR + RAS granules (RAG) in DMED. We then validated these findings in DMED rat models to examine the effects of RAG on histopathological changes in the corpus cavernosum and key proteins involved in hypoxia-related pathways. The overall study design is summarized in **Figure 1**.

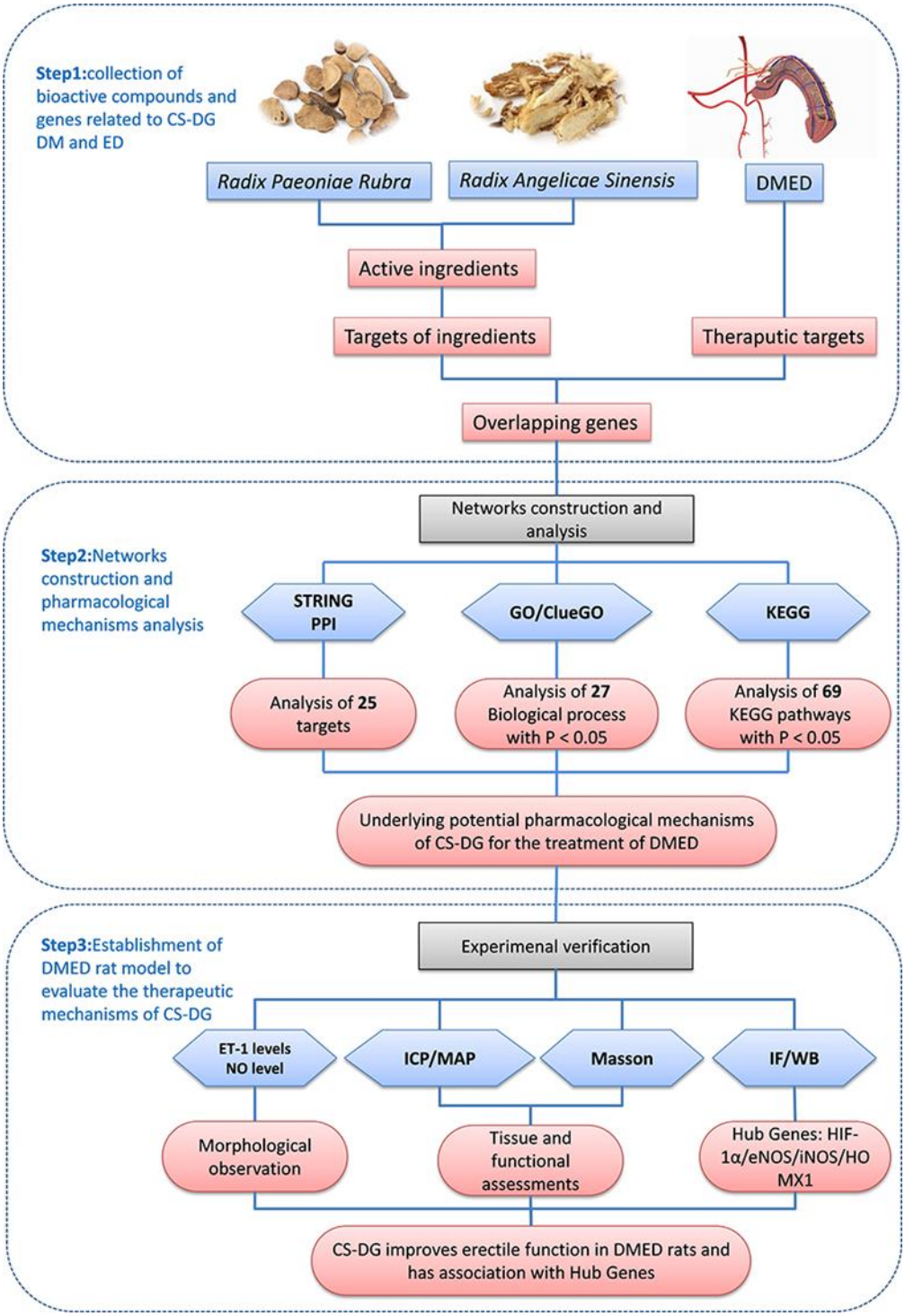

Figure 1. Flowchart showing the network pharmacology method used in this study and its experimental validation

Materials and Methods

Identification of active components of RAG and target prediction

The active compounds of Radix Paeoniae Rubra (RPR) and Radix Angelicae Sinensis (RAS) were retrieved from the Traditional Chinese Medicine Systems Pharmacology (TCMSP) database (http://lsp.nwu.edu.cn/tcmsp.php), a widely used resource for network pharmacology research linking traditional Chinese medicine to modern biomedical data [23]. To identify biologically relevant compounds, we applied thresholds of oral bioavailability (OB) ≥ 30% and drug-likeness (DL) ≥ 0.05.

Target identification for RAG compounds

Potential targets of the active RAG compounds were also obtained from the TCMSP database. UniProt (http://www.uniprot.org) was subsequently used to standardize protein names to gene symbols to facilitate data integration and analysis.

DMED-associated targets

Targets related to diabetes mellitus-induced erectile dysfunction (DMED) were retrieved from GeneCards (https://www.genecards.org/), OMIM (https://www.omim.org/), and PharmGKB (https://www.pharmgkb.org/). Search terms included "Diabetes Mellitus" and "Erectile Dysfunction." Results from the three databases were merged, duplicates removed, and consolidated to generate a comprehensive DMED target set.

Identification of common targets and network construction

Common targets shared by RAG compounds and DMED were identified using R software (v3.6.4). Protein-protein interaction (PPI) networks were constructed using the STRING database (https://string-db.org/) with a minimum interaction confidence score of 0.4. Target frequency was analyzed in R, and results were visualized in histogram format. A drug-ingredient-disease-target interaction network was generated using Cytoscape 3.7.1 (https://cytoscape.org/), with nodes representing drugs, compounds, diseases, and targets, facilitating visualization of complex relationships.

Functional enrichment and pathway analyses

Gene Ontology (GO) and Kyoto Encyclopedia of Genes and Genomes (KEGG) pathway enrichment analyses of core targets were performed using OmicShare tools (www.omicshare.com/tools). Statistical significance was set at $P < 0.05$. Results were presented as bubble plots, bar graphs, and circular enrichment diagrams to interpret the biological functions and pathways through which RAG may influence DMED.

Molecular docking

Three-dimensional crystal structures of core targets—BDNF (PDB ID: 1B8M, 2.75 Å), CASP3 (3KJF, 2.00 Å), CAT (1DGH, 2.00 Å), CRP (3PVN, 1.98 Å), INS (6SOF, 4.30 Å), and HMOX1 (1S13, 2.29 Å)—were downloaded from the Protein Data Bank. Chemical structures of major RAG compounds, including (+)-catechin, oleic acid, butylated hydroxytoluene, and β-sitosterol, were obtained from PubChem (https://pubchem.ncbi.nlm.nih.gov), converted to 3D structures, and energy-minimized using MOE 2015.10 software. Target proteins were prepared by dehydration, hydrogen addition, and identification of active binding sites via Site Finder or natural ligand atoms. Molecular docking simulations were performed in MOE using default parameters. Binding free energy (ΔGb) was calculated, and the pose with the lowest binding energy was selected to evaluate the potential interactions between RAG compounds and core targets, providing insights into the molecular mechanisms underlying the therapeutic effects of RAG on DMED.

Single-cell sequencing analysis

To examine the involvement of HIF1A in erectile dysfunction, single-cell RNA sequencing data were obtained from the GEO database (GSE206528) [17]. The dataset included five penile tissue samples: three from non-tumor regions of penile cancer resections serving as controls with normal erectile function, and two from DMED patients who underwent artificial cavernous implantation. The DMED patients had type 1 diabetes for over ten years and maintained well-controlled glycemia preoperatively. Data preprocessing, clustering, and visualization were performed using the Seurat package, and marker genes were identified using CellMarker 2.0. Comparisons of cell composition, signature gene expression, and HIF1A levels were conducted between the control and DMED groups. According to Chinese regulations (Article 32, Item 1, 2023), use of publicly available, ethically approved data qualifies for exemption from additional ethical approval.

Preparation of RAG

RAG was composed of Radix Paeoniae Rubra (RPR, 15 g) and Radix Angelicae Sinensis (RAS, 15 g) granules, sourced from Zhejiang Huisong Pharmaceutical Co., Ltd. (batch numbers ZBT1-24-80 and ZBT1-24-134). RPR is derived from dried roots of *Paeonia lactiflora* Pall., while RAS comes from dried roots of *Angelica sinensis* (Oliv.) Diels. All granules were prepared according to the 2015 Chinese Pharmacopoeia, stored in cool and dry

conditions, and quality-assessed by Professor Chen Hongshu (Zhejiang Hospital of Traditional Chinese Medicine).

Chemical characterization of RAG

Active components of RAG were analyzed using UHPLC-QTOF-MS/MS (Waters ACQUITY system, BEH C18 column, 100 × 2.1 mm, 1.7 μm). The mobile phase consisted of 0.1% formic acid in acetonitrile (A) and water (B) with gradient elution (0–2 min: 99% B; 2–12 min: 55–99% B; 12–17 min: 15–55% B). Injection volume was 1 μL, flow rate 0.3 mL/min, column temperature 30 °C. MS analysis was performed on a Waters G2 QTOF™ system.

Animals and housing conditions

Male Sprague Dawley rats (8 weeks old, 180–200 g) were obtained from Zhejiang Chinese Medicine University (SYXK 2021). Rats were housed under SPF conditions (24 ± 2 °C, 45–55% humidity, 12 h light/dark cycle) with ad libitum access to food and water. Experiments were conducted according to NIH guidelines and approved by the university's Animal Care and Use Committee (20220411–13).

DMED model induction and RAG administration

After one week of acclimation, 30 rats were fed a high-fat diet for one month and then injected intraperitoneally with streptozotocin (60 mg/kg) after 12 h fasting to induce diabetes. Ten control rats received citrate buffer. Fasting glucose was measured after 72 h, and 25 rats with glucose >16.7 mmol/L were classified as diabetic. After eight weeks, the apomorphine (APO)-induced erection test (100 μg/kg, s.c.) was used to identify 20 DMED rats with erectile dysfunction, randomly divided into model (n=10) and RAG-treated groups (n=10). RAG was administered orally at 5.4 g/kg/day (equivalent to 17.8 g/kg crude drug) for four weeks, while control groups received saline. Body weight and fasting glucose were measured weekly.

Evaluation of endothelial function

Serum ET-1 levels were measured using the EU0205 kit (Wuhan Fine Biotech) to assess endothelial function. Plasma was separated by centrifugation at 1000 rpm for 15 min at 2–8 °C. NO levels, an indicator of endothelial health, were measured using the A013-2-1 kit (Nanjing Jiancheng Bioengineering), following manufacturer instructions.

Assessment of erectile function

After treatment, rats were anesthetized with sodium pentobarbital. Carotid artery cannulation was used to monitor systemic blood pressure. The cavernous nerves were exposed, and electrical stimulation (5 V, 15 Hz, 5 ms pulse width, 60 s duration, 5 min interval) was applied. ICP and MAP were recorded using the MP160 system (Biopac), and erectile function was quantified using maximum ICP, max ICP/MAP ratio, and ICP rise rate.

Morphological evaluation

Following the assessment of erectile function, penile tissues were harvested from anesthetized rats. The corpus cavernosum was divided into two portions: one segment was fixed in 4% paraformaldehyde for histological analysis, and the other was rapidly frozen in liquid nitrogen and stored at −80 °C for subsequent biochemical and molecular studies. Rats were euthanized immediately after tissue collection.

Histological changes in the corpus cavernosum were evaluated using Masson's trichrome staining (Solarbio, Beijing, China) to determine the relative proportion of smooth muscle to collagen fibers. Images were captured with a NanoZoomer S60 digital slide scanner (HAMAMATSU, Shizuoka, Japan), with smooth muscle appearing red and collagen fibers blue. Quantitative analysis of stained sections was performed using ImagePro Plus 6.0 software (Media Cybernetics, Rockville, MD, USA). Additionally, apoptotic changes in cavernous smooth muscle cells were assessed by TUNEL staining (Share-bio, Shanghai, China). Fluorescent images identified nuclei in blue and apoptotic cells in red, enabling evaluation of tissue integrity and cellular apoptosis under DMED conditions and following RAG treatment.

Immunofluorescence and western blot analysis

To determine the expression and localization of key proteins implicated in DMED pathology, immunofluorescence (IF) staining was performed on corpus cavernosum tissue sections. Sections were incubated overnight (18 h) at 4 °C with primary antibodies against HIF-1α, eNOS, iNOS, HMOX1, and β-actin (1:200). Following washing, sections were exposed to Alexa Fluor 488-conjugated secondary antibodies (1:500), and nuclei were counterstained with DAPI. Fluorescence images were analyzed using ImagePro Plus 6.0.

For quantitative protein expression analysis, Western blotting (WB) was conducted. Corpus cavernosum tissue (approximately 100 mg) was homogenized in RIPA buffer on ice for 30 minutes, and total protein content was measured using a BCA assay (Beyotime Co., Ltd., China). Equal amounts of protein (50 μg) were separated via SDS-PAGE and transferred to PVDF membranes (Bio-Rad, Hercules, CA, USA). Membranes were blocked with 5% skim milk for 2 h at room temperature and incubated overnight with primary antibodies against HIF-1α, eNOS, iNOS, HMOX1, and β-actin (1:1000). After washing, membranes were incubated with the appropriate secondary antibodies for 1.5 h. Protein bands were detected using enhanced chemiluminescence (ProteinSimple, USA) and quantified using ImageJ (v1.48). β-actin served as the loading control, and all assays were performed in triplicate.

Statistical analysis

All measurements are expressed as mean ± standard deviation (SD). Differences among groups were analyzed using one-way ANOVA followed by Tukey's post-hoc test (SPSS 26.0). A P-value < 0.05 was considered statistically significant. Graphs were generated using GraphPad Prism 8.0.

Results and Discussion

Active compound screening of RAG

A total of 119 compounds were identified in RPR and 125 in RAS. Applying the screening criteria (oral bioavailability ≥ 30% and drug-likeness ≥ 0.05), 71 pharmacologically active components were selected **(Table 1)**. Key active compounds included paeonin, paeoniflorgenone, camphoric acid, senkyunolide D, 2-valerylbenzoic acid, and sedanolide. These compounds were subsequently analyzed for their potential contributions to the therapeutic effects of RAG in DMED.

Table 1. Radix Angelicae Sinensis-Angelica Sinensis Bio-Active Ingredients Screened in TCMSP

	MOL NO.	Bio-Active Ingredients	OB%	DL
RPR	MOL007015	8-debenzoylpaeonidanin_qt	129.3	0.15
RPR	MOL007029	Paeonin,b_qt	105.45	0.08
RPR	MOL001935	(3aR,6S,7aR)-6-hydroxy-6-methyl-3-methylene-3a,4,7,7a -tetrahydrobenzofuran-2,5-dione	97.79	0.08
RPR	MOL001918	Paeoniflorgenone	87.59	0.37
RPR	MOL000244	()-Borneol	81.8	0.05
RPR	MOL007027	paeonin,a_qt	73.79	0.09
RPR	MOL007031	Paeonin,c_qt	72.7	0.09
RPR	MOL001925	Paeoniflorin_qt	68.18	0.4
RPR	MOL007016	Paeoniflorigenone	65.33	0.37
RPR	MOL006996	1-o-beta-d-glucopyranosy lpaeonisuffrone_qt	65.08	0.35
RAS	MOL008286	()-Camphoric acid	99.13	0.07
RAS	MOL002144	Senkyunolide-D	79.13	0.1
RAS	MOL008265	2-valerylbenzoic acid	78.26	0.06
RAS	MOL008259	2,6-di(phenyl) thiopyran-4-thione	69.13	0.15
RAS	MOL008252	Senkyunolide	68.28	0.07
RAS	MOL002098	3-Butylidene-7- hydroxyphthalide	62.68	0.08
RAS	MOL008251	Sedanolide	62.46	0.07

RAS	MOL002033	cis-THUJOPSENE	56.43	0.12
RAS	MOL008256	(3S)-3-butyl-3H- isobenzofuran-1-one	55.05	0.07
RAS	MOL008285	FERULIC ACID (CIS)	54.97	0.06

Note: Sort by OB value only list the top 10 compounds per drug.
Abbreviations: RPR, Radix Paeoniae Rubra; RAS, Radix Angelicae Sinensis.

Targets of bioactive compounds in RAG

Through analysis using the TCMSP database, a total of 458 potential targets of the bioactive compounds in RAG were identified. Notably, succinic acid, oleic acid, methylbutenol, α-terpineol, and quercetin were found to interact with 33, 30, 30, 19, and 77 targets, respectively, suggesting their prominent role in mediating the therapeutic effects of RAG. Target protein names were standardized using the UniProt database, and duplicates or invalid entries were excluded. Ultimately, 107 valid target genes corresponding to the active compounds of RAG were retained for further analysis.

Identification of DMED-related targets and construction of the drug–ingredient–gene network

Disease-associated targets for diabetes mellitus and erectile dysfunction were retrieved from OMIM, GeneCards, and PharmGKB databases, yielding 1000 and 953 candidate targets, respectively, using a relevance score threshold of ≥ 10. Mapping the targets of RAG's active compounds against the disease-associated targets revealed 25 overlapping genes, which were considered critical targets for RAG's intervention in DMED **(Figure 2a)**.

To visualize the complex interactions between the herbal compounds and disease-related targets, a drug–ingredient–gene (D-I-G) network was constructed using Cytoscape 3.7.1. The network comprised 20 nodes representing active compounds in RAG and 25 nodes representing disease targets **(Figure 2b)**. Among these, NOS, CAT, CASP3, HMOX1, SOD, and MPO exhibited higher connectivity, indicating their central roles in the pathogenesis of DMED and their potential as key targets of RAG treatment.

a)

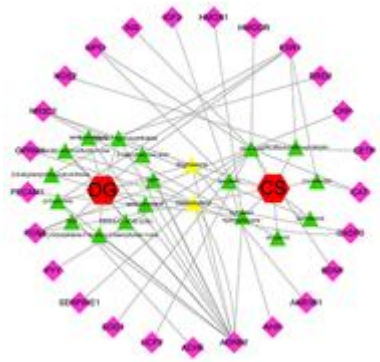

b)

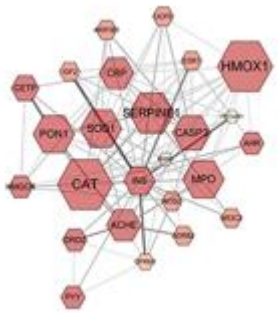

c)

d)

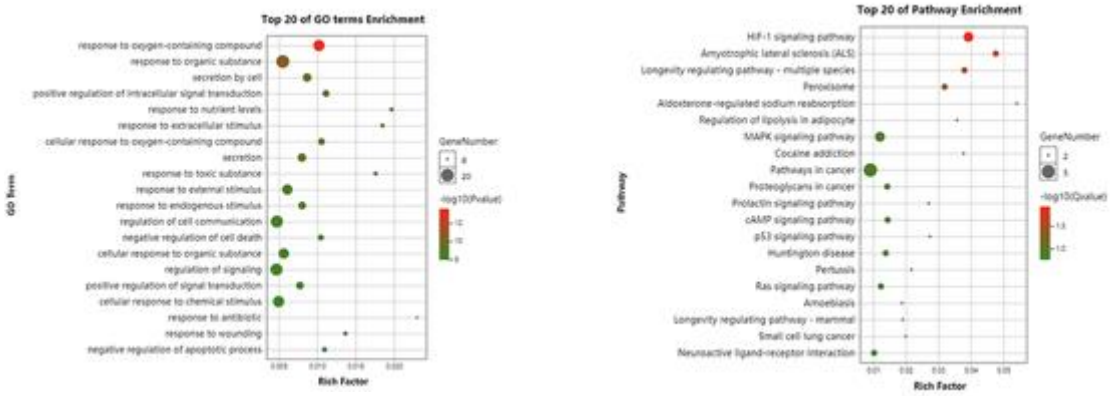

e) f)

Figure 2. Drug-disease gene screening and bioinformatics analysis. (a) We found 25 genes shared between the drug and the disease. (b) A network diagram shows relationships: 25 purple nodes for shared genes, 20 green for RAG ingredients, 2 yellow for shared RPR and RAS ingredients, and an Orange node for RAG. Lines indicate possible interactions. (c) The PPI network for RAG's bioactive ingredients against DMED is shown, with thicker, darker lines for stronger interactions and larger, darker red nodes for more connected targets. (d) A bar graph displays the interaction frequency of the 25 most common target proteins in the PPI network, with the number of connections on the x-axis and the proteins on the y-axis. (e) The GO tool analysis shows the 25 DMED-related genes' enrichment in biological processes, with factors on the x-axis, categories on the y-axis, bubble size for gene count, and color intensity for significance. (f) KEGG pathway analysis indicates the genes' enrichment in signaling pathways, with factors on the x-axis, pathways on the y-axis, bubble size for gene count, and color intensity for significance.

Protein–protein interaction (PPI) network of drug–disease targets

A PPI network for the 25 overlapping targets between RAG and DMED was constructed using the STRING database, consisting of 25 nodes and 112 edges **(Figure 2c)**. The R software was used to calculate the interaction frequency of each target, which was visualized in a bar chart **(Figure 2d)**. Key proteins with higher interaction frequencies included INS, CAT, BDNF, CASP3, CRP, and HMOX1, with HMOX1 occupying the central hub of the network, indicating its potential significance in mediating the therapeutic effects of RAG.

Enrichment analysis and core pathways of RAG against DMED

Gene Ontology (GO) enrichment analysis revealed that the 25 common targets were primarily associated with biological processes such as vasodilation, regulation of protein secretion, apoptosis, oxidative and antioxidative processes, and responses to hypoxia ($P < 0.01$; **(Figure 2e)**). These findings suggest that RAG may exert therapeutic effects in DMED by modulating multiple interconnected biological processes.

KEGG pathway enrichment analysis further demonstrated that these targets were predominantly involved in signaling pathways including HIF-1, MAPK, cAMP, and Ras **(Figure 2f and Table 2)**. The visualization indicated that pathways represented by larger red nodes corresponded to greater enrichment and higher significance, suggesting that RAG may influence multiple critical pathways to ameliorate DMED. Collectively, these analyses highlight the multi-target and multi-pathway nature of RAG's mechanism of action in treating DMED.

Table 2. Result of Target Pathway Enrichment (Top 20)

Pathway ID	Pathway Name	Count	P value	Gene Name
ko04066	HIF-1 signaling pathway	4	9.94E-05	*NOS2/HOMX1/SERPINE1/INS*
ko05014	Amyotrophic lateral sclerosis (ALS)	3	0.000467	*CAT/SOD1/CASP3*
ko04213	Longevity regulating pathway - multiple species	3	0.000907	*CAT/SOD1/INS*
ko04146	Peroxisome	3	0.001501	*NOS2/CAT/SOD1*

ko04960	Aldosterone-regulated sodium reabsorption	2	0.003664	*NR3C2/INS*
ko05030	Cocaine addiction	2	0.007403	*DRD2/BDNF*
ko04010	MAPK signaling pathway	4	0.008029	*CASP3/IGF2/BDNF/INS*
ko04923	Regulation of lipolysis in adipocyte	2	0.008236	*ADRB2/INS*
ko05200	Pathways in cancer	5	0.009459	*NOS2/ESR1/HOMX1/CASP3/IGF2*
ko04115	p53 signaling pathway	2	0.013706	*SERPINE1/CASP3*
ko04024	cAMP signaling pathway	3	0.013817	*DRD2/ADRB2/BDNF*
ko04917	Prolactin signaling pathway	2	0.014066	*ESR1/INS*
ko05205	Proteoglycans in cancer	3	0.014177	*ESR1/CASP3/IGF2*
ko05016	Huntington disease	3	0.015477	*SOD1/CASP3/BDNF*
ko04014	Ras signaling pathway	3	0.02089	*IGF2/BDNF/INS*
ko05133	Pertussis	2	0.021227	*NOS2/CASP3*
ko05222	Small cell lung cancer	2	0.024807	*NOS2/CASP3*
ko04211	Longevity regulating pathway - mammal	2	0.027162	*CAT/INS*
ko05146	Amoebiasis	2	0.027643	*NOS2/CASP3*
ko04933	AGE-RAGE signaling pathway in diabetic complications	2	0.03162	*SERPINE1/CASP3*

Molecular docking analysis

Molecular docking simulations were performed to evaluate the binding affinity between the main active compounds of RAG and key target proteins. The docking scores of oleic acid with BDNF, CAT, CRP, and INS were −6.39, −10.86, −6.91, and −107.93 kcal/mol, respectively. Meanwhile, the binding energies of beta-sitosterol with CASP3, (+)-catechin with CAT, and butylated hydroxytoluene with HMOX1 were −6.37, −7.98, and −5.57 kcal/mol, respectively **(Table 3)**.

The docking results revealed multiple interaction modes, including hydrogen bonding, H-π interactions, and π-π stacking. Several amino acid residues—such as His75, Arg8112, Phe207, Lys8114, Tyr8507, and Leu8552—participated in these interactions with the target proteins. The detailed binding conformations between each compound and hub protein are illustrated in **Figures 3a–3g**. **Table 3** summarizes the docking affinities between RAG's active ingredients and the corresponding target genes, indicating stable binding and potential pharmacological relevance.

Table 3. Result of Target Pathway Enrichment (Top 20)

Gene name	PDB ID	Herbs	Compound			H-Bonds		π-Interactions	
			Name	PubChem CID Compound	ΔGb	Type Amino Acid	Type Amino Acid	Amino Acid	Amino Acid
BDNF	1B8M	RPR	Oleic acid	445639	−6.3901	-	-	-	-
CAPS3	3KJF	RPR and RAS	Beta-sitosterol	12303645	−6.3707	-	-	-	-
CAT	1DGH	RPR and RAS	(+)-catechin	9064	−7.9781	-	-	pi-pi	His 75
CAT	1DGH	RPR	Oleic acid	445639	−10.8577	H-donor H-acceptor	Arg B-112 Arg B-112	-	-
CRP	3VPN	RPR	Oleic acid	445639	−6.9114	H- acceptor	Lys *B*-114	-	-
HMOX1	1S13	RPR	butylated hydroxytoluene	31404	-5.5655			H-pi	Phe 207
INS	6SOF	RPR	Oleic acid	445639	-107.9273	H-donor H-donor H-acceptor H-acceptor	Leu *E*-552 Leu *B*-552 Try *B*-507 Try *E*-507	-	-

Abbreviations: RPR, Radix Paeoniae Rubra; RAS, Radix Angelicae Sinensis.

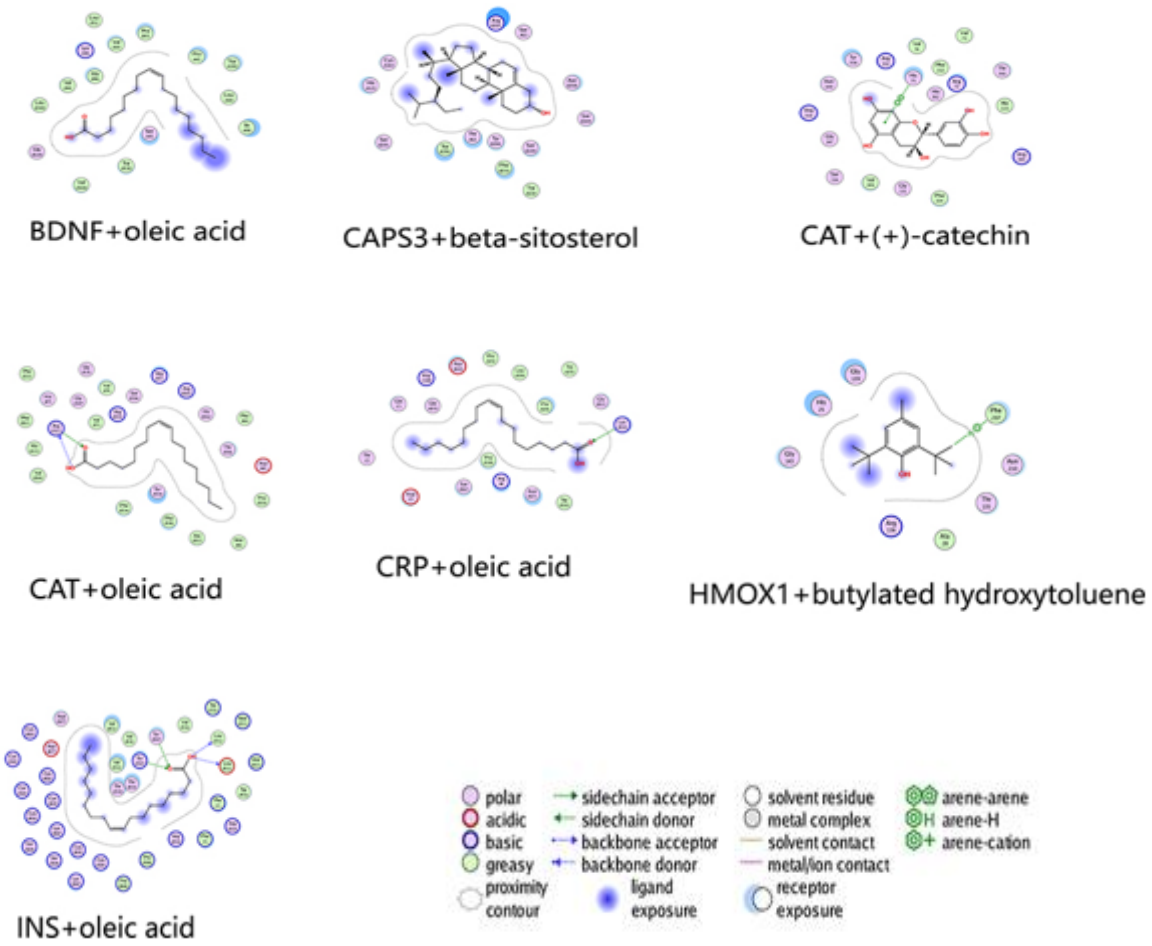

Figure 3. conducted molecular docking to explore the interactions between RAG's key bioactive compounds and their primary protein targets. Four representative compounds were evaluated against six critical targets. Oleic acid docking with BDNF, CAT, CRP, and INS is shown in panels (a), (d), (e), and (f), respectively. Docking of beta-sitosterol with CASP3, (+)-catechin with CAT, and butylated hydroxytoluene with HMOX1 are depicted in panels (b), (c), and (g). The analyses revealed multiple binding interactions, including hydrogen bonds and π-related interactions, highlighting potential molecular mechanisms through which RAG may influence DMED-associated proteins.

Single-cell transcriptomic profiling in ED

To investigate cellular heterogeneity in erectile tissue, we performed single-cell RNA sequencing and applied unsupervised clustering, visualized through UMAP. This approach revealed distinct populations including endothelial cells (C0, C2), fibroblasts (C1, C5, C9), smooth muscle cells (C3, C6, C10), vascular smooth muscle cells (C4), macrophages (C7), and T cells (C8) **(Figures 4a and 4b)**.

Marker gene analysis using t-SNE maps confirmed cell type identity, with VWF marking endothelial cells, DCN marking fibroblasts, ACTA2 marking smooth muscle cells, TAGLN marking vascular smooth muscle cells, CD86 marking macrophages, and CD3D marking T cells **(Figure 4c)**. Importantly, HIF1A expression differed notably between cells from diabetic versus non-diabetic samples **(Figure 4d)**, and its levels varied among the identified cell populations **(Figures 4e and 4f)**. These results suggest that HIF1A may play a critical role in endothelial and smooth muscle dysfunction associated with DMED.

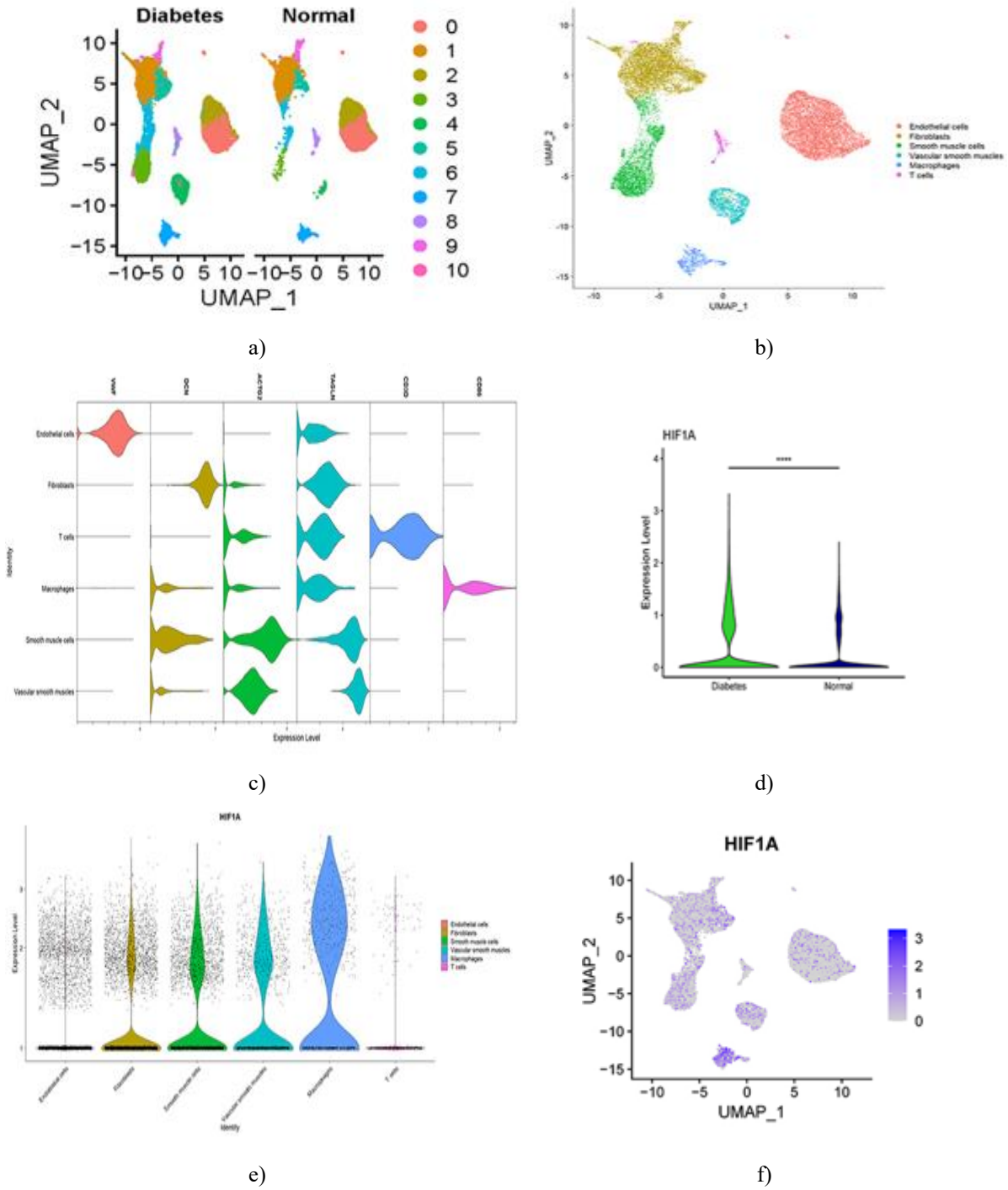

Figure 4. Single-cell sequencing revealed the global expression profile of diabetes mellitus-induced erectile dysfunction (DMED) patients. (a) The tSNE plots visually represent the cellular heterogeneity among the cavernosal cells from the five donors, offering a two-dimensional projection that captures the complex cellular relationships. (b) Post cell annotation, the tSNE plots are color-coded to distinguish between different cell types, providing a clear visual distinction of the cellular composition within the samples. (c) Utilize CellMarker 2.0 to identify cellular markers. (d) This comparative expression analysis of HIF1A is presented to highlight any significant disparities between the two groups, which could be indicative of the role of HIF1A in the development of erectile dysfunction in type 1 diabetes patients. (e) The expression patterns of HIF1A across the entire dataset of cavernosal cells are depicted, illustrating how HIF1A expression varies within the cellular populations. (f) The tSNE profiles of all cavernosal cells (CC cells) are annotated with HIF1A expression levels, offering a comprehensive view of the distribution and potential clustering of cells based on their HIF1A expression profiles.

Single-cell transcriptomic profiling in DMED

We performed single-cell RNA sequencing to examine cellular heterogeneity in the penile tissue of DMED patients. Using t-SNE dimensionality reduction, we visualized the distribution of cells across the samples **(Figure 4a)**. Cell populations were annotated based on marker gene expression, identifying endothelial cells (C0, C2), fibroblasts (C1, C5, C9), T cells (C8), macrophages (C7), smooth muscle cells (C3, C6, C10), and vascular smooth muscle cells (C4) **(Figure 4b)**. CellMarker 2.0 supported the assignment of cell-type-specific markers, including VWF for endothelial cells, DCN for fibroblasts, ACTA2 for smooth muscle, TAGLN for vascular smooth muscle, CD86 for macrophages, and CD3D for T cells **(Figure 4c)**. HIF1A expression was then assessed across all cell types, revealing notable differences between diabetic and control samples **(Figures 4d–4f)**, suggesting its potential involvement in DMED pathophysiology.

Chemical analysis of RAG

The chemical composition of RPR and RAS granules was determined by UHPLC-QTOF-MS/MS. Data processing was conducted with SCIEX OS software, and compound identification relied on first-order accurate mass, isotope patterns, MS/MS fragmentation, and the TCM MS/MS reference library. Overall, 12 compounds were detected in positive ion mode and 28 in negative ion mode, predominantly comprising glycosides, esters, and organic acids. Several of these compounds corresponded to those previously reported in TCMSP database screenings for RPR and RAS.

RAG effects on physiological parameters and endothelial function

Throughout the four-week study, body weights of RAG-treated DMED rats did not significantly differ from untreated DMED rats ($P > 0.05$). Blood glucose measurements showed that RAG administration partially reduced fasting glucose levels on days 14, 21, and 28 compared to untreated DMED rats ($P < 0.01$), though levels remained above those of healthy controls **(Figures 5a and 5b)**. Serum assays indicated a marked reduction of NO and an elevation of ET-1 in untreated DMED rats ($P < 0.01$; **(Figures 5c and 5d)**), consistent with endothelial dysfunction. Treatment with RAG reversed these trends, increasing NO availability and lowering ET-1 concentrations ($P < 0.01$), indicating a restoration of endothelial function.

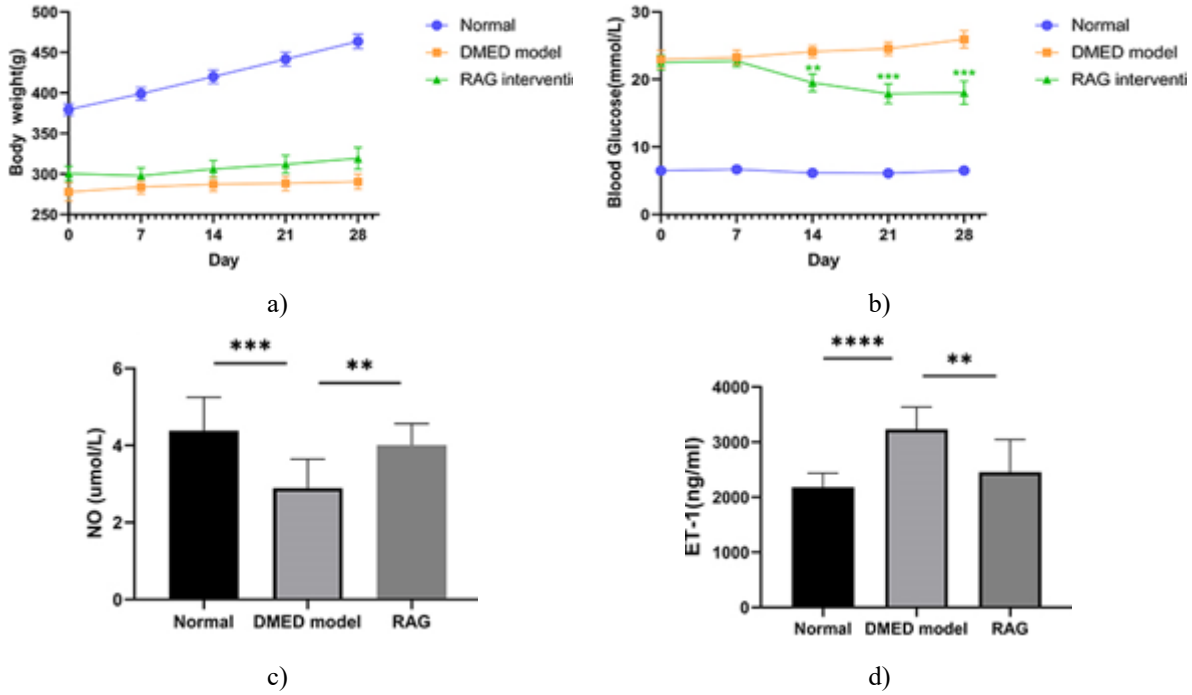

Figure 5. Impact of RAG on Physiological Parameters and Endothelial Function in DMED Rats

Panels (a) and (b) depict weekly measurements of body weight and fasting blood glucose, respectively, in all experimental groups following the initiation of treatment. Blue dots indicate the control group, orange dots represent the DMED model group, and green dots denote the RAG-treated group. Panels (c) and (d) show the

serum concentrations of nitric oxide (NO) and endothelin-1 (ET-1). Data are expressed as mean ± SD. **p < 0.01, ***p < 0.001, ****p < 0.0001 indicate statistical significance compared with the relevant group.

RAG improves erectile function in DMED rats

Erectile function was assessed by measuring intra-cavernous pressure (ICP) and mean arterial pressure (MAP) under electrical stimulation at 0 and 5 V **(Figure 6a)**. **Figures 6b–6d** present the maximum ICP (max ICP), the max ICP/MAP ratio, and the ICP slope (rate of pressure rise) for each group. DMED rats showed a significant reduction in the max ICP/MAP ratio compared with controls (P < 0.01), confirming successful induction of erectile dysfunction. Treatment with RAG notably enhanced the max ICP/MAP ratio and ICP slope, suggesting a restoration of erectile function in DMED rats.

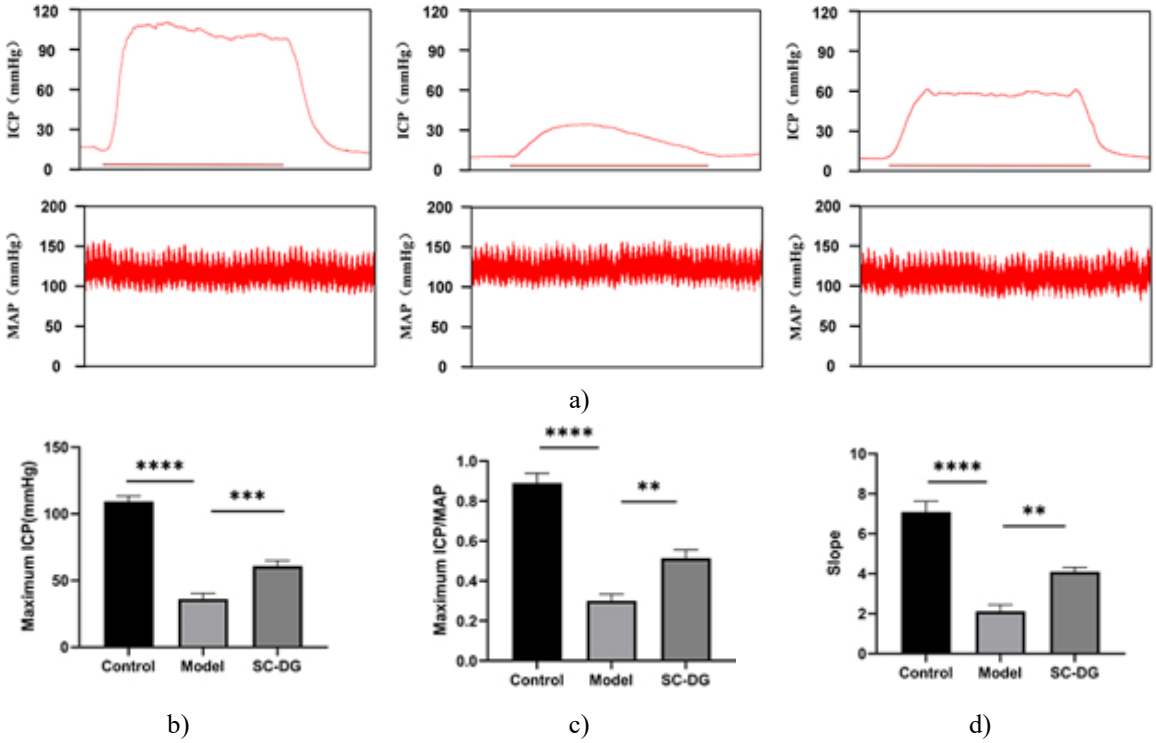

Figure 6. ICP and MAP Measurements in Experimental Rats

Panel (a) presents the ICP and MAP recordings over time for each group, with the y-axis representing pressure (mmHg) and the x-axis representing time; the horizontal line indicates the duration of electrical stimulation. Panels (b–d) show quantitative analyses of maximal ICP, maximal ICP/MAP ratio, and the mean ICP rise rate (slope) following stimulation (n = 5 per group). Statistical significance is indicated as **p < 0.01, ***p < 0.001, and ****p < 0.0001.

Histopathological changes in penile tissue

Examination of penile tissue from the DMED group revealed substantial endothelial swelling and plasma membrane damage, in contrast to the intact architecture observed in controls. Cavernous tissue in the DMED rats displayed irregularly distributed endothelial and smooth muscle cells with disrupted structural integrity. Collagen deposition was markedly elevated, reflecting pronounced fibrosis, and the smooth muscle to collagen ratio was significantly reduced compared with control animals (P < 0.001). By comparison, RAG-treated rats showed restoration of endothelial cell and smooth muscle content and a significant increase in the smooth muscle to collagen ratio relative to the DMED model group (P < 0.05), suggesting that RAG mitigates DMED-induced structural abnormalities **(Figure 7a)**. Tunel staining further demonstrated a substantial rise in apoptotic cells in the cavernous tissue of DMED rats, whereas RAG treatment significantly reduced apoptosis, indicating a protective effect against diabetes-induced cellular damage **(Figure 7b)**.

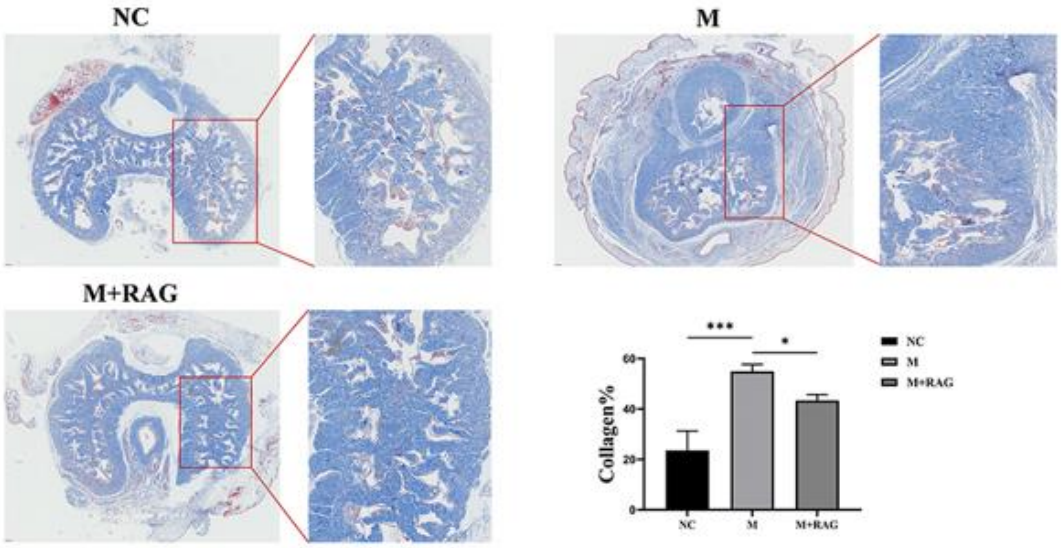

a)

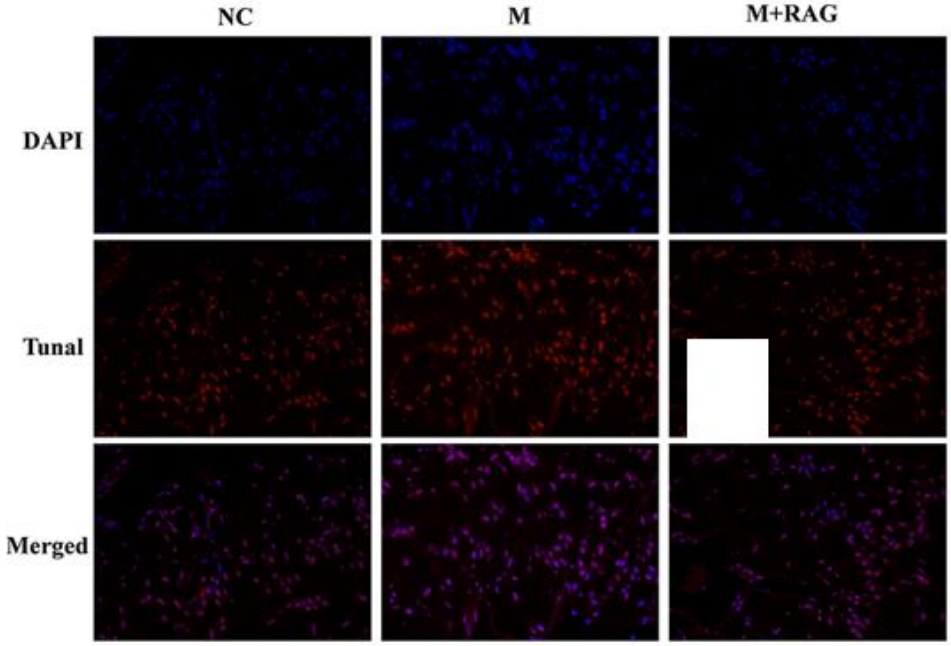

b)

Figure 7. Penile Tissue Morphology and Apoptosis Analysis

(a) Representative Masson's trichrome-stained sections of the corpus cavernosum (×100) are shown. Smooth muscle fibers are highlighted in red, while collagen fibers are stained blue. Compared to DMED rats, those receiving RAG treatment exhibited increased smooth muscle content and reduced collagen deposition, indicating an improvement in tissue structure.

(b) TUNEL staining demonstrates the level of apoptosis in corporal smooth muscle cells. Apoptotic cells emit red fluorescence, and cell nuclei are counterstained with DAPI (blue). RAG intervention markedly decreased the number of apoptotic cells relative to the untreated DMED group. Statistical differences are indicated by $*p < 0.05$ and $***p < 0.001$.

Effects of RAG on core hypoxia-related proteins in DMED rats

To investigate the molecular mechanisms underlying RAG's protective effects, we focused on key hypoxia-related proteins identified from the PPI network and molecular docking analyses. The expression of HIF-1α, eNOS, iNOS, and HMOX1 in penile tissues was evaluated by immunofluorescence and Western blotting **(Figures 8a and 8b)**. DMED rats exhibited significantly elevated HIF-1α levels ($P < 0.05$) and decreased expression of eNOS, iNOS, and HMOX1 ($P < 0.01$, < 0.01, and < 0.05, respectively), compared with controls. Treatment with RAG

restored eNOS and iNOS levels ($P < 0.05$ and < 0.01) and suppressed HIF-1α expression ($P < 0.05$). Immunofluorescence images corroborated these changes, suggesting that RAG mitigates hypoxia-induced damage and improves endothelial and smooth muscle function in DMED penile tissue.

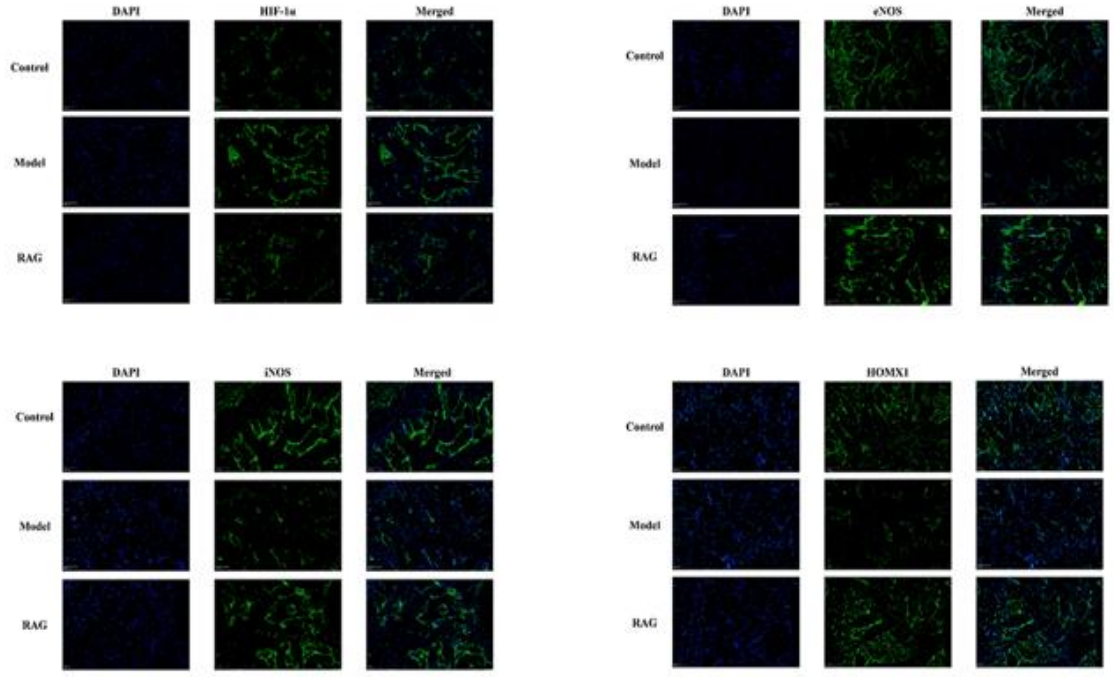

a)

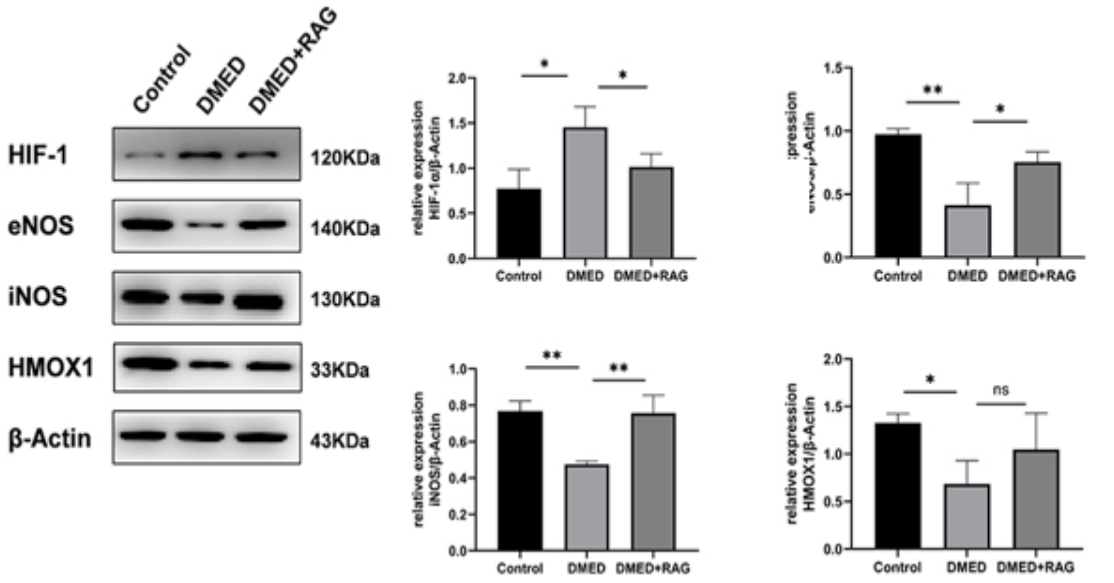

b)

Figure 8. RAG treatment regulates the expression of hub genes in DMED rat corpus cavernosum. (a) Representative images of immunofluorescent staining of cavernosal tissue with anti-HIF-1α, anti-eNOS, anti-iNOS, and anti-HMOX1 in various groups. (b) HIF-1α, eNOS, iNOS, and HMOX1 protein expression in cavernous tissues from the three groups were determined by Western blotting. Error bars: mean SD; n = 5–6 in each group. NS: not significant ($p \geq 0.05$), *$p < 0.05$, **$p < 0.01$.

The pathophysiology of DMED is multifactorial and remains incompletely understood, posing challenges for effective clinical management. Current treatments, including PDE5 inhibitors, often fail to achieve optimal outcomes in diabetic patients, highlighting the need for alternative therapeutic targets. DMED is associated with oxidative stress, accumulation of advanced glycation end products, endothelial dysfunction, neuropathy, and

fibrotic changes in the penile tissue [24]. From the perspective of traditional Chinese medicine, diabetes is linked to a deficiency of both qi and yin, accompanied by blood stasis and toxin accumulation, which are thought to contribute to vascular complications. Accordingly, RPR and RAS are frequently prescribed to promote blood circulation and resolve stasis, and their combined use is believed to potentiate therapeutic efficacy for conditions involving collateral obstruction. Prior studies have also demonstrated that this combination can protect against neurodegeneration, reduce high glucose–induced renal epithelial–mesenchymal transition, mitigate advanced glycation end product–mediated renal injury, and modulate oxidative stress [19, 25, 26].

Given the multicomponent nature of traditional Chinese medicine, dissecting the mechanisms of RAG is inherently complex. Here, network pharmacology facilitated systematic identification of potential targets, which were subsequently validated experimentally. Our analysis revealed that the principal bioactive compounds in RAG include paeoniflorin, albiflorin, paeoniflorigenone, senkyunolide, beta-sitosterol, oleic acid, and sedanolide. Among these, beta-sitosterol, oleic acid, butylated hydroxytoluene, and (+)-catechin emerged as core nodes in the drug–target network and exhibited strong binding affinity to hub targets in molecular docking studies. These findings suggest that these compounds play a critical role in mediating RAG's therapeutic effects in DMED.

Previous research has highlighted the ability of RAG constituents to enhance vascular endothelial function, improve microcirculation, reduce blood viscosity and vascular resistance, alleviate arteriole spasm, and decrease vascular inflammation [27–29]. Endothelial injury is a key contributor to DMED, and in our study, RAG treatment increased serum NO levels while reducing ET-1 concentrations, indicating improved endothelial function. Additionally, certain RAG components demonstrated hypoglycemic effects, supporting vascular health while addressing underlying metabolic abnormalities [30, 31]. In our rat model, fasting blood glucose was significantly reduced following 14 days of RAG treatment, although it did not normalize completely.

Integrating the 25 shared drug–disease targets with PPI network and KEGG pathway enrichment analyses, we identified that RAG potentially exerts its effects through multiple signaling pathways, including HIF-1, MAPK, cAMP, and Ras. Hub proteins, such as BDNF, CASP3, CAT, CRP, INS, and HMOX1, were associated with key bioactive compounds, including beta-sitosterol, oleic acid, butylated hydroxytoluene, and (+)-catechin, as confirmed by molecular docking.

HIF-1α overexpression is strongly implicated in DMED pathogenesis, promoting smooth muscle apoptosis and fibrosis under hypoxic conditions [32, 33]. Inhibition of HIF-1α restores eNOS activity and NO production, which are essential for maintaining penile erection. Our results indicate that RAG reduces HIF-1α expression and enhances eNOS and iNOS levels, thereby mitigating hypoxic stress and improving erectile function.

HMOX1, identified as a central node in the PPI network, acts as a stress-responsive enzyme that degrades heme into biliverdin, carbon monoxide, and iron, protecting cells from apoptosis [34]. As a downstream effector of HIF-1α, HMOX1 helps maintain tissue homeostasis under hypoxic, ischemic, and inflammatory conditions [35–37]. Recent studies demonstrate that upregulation of HMOX1 can alleviate endothelial cell injury and oxidative stress in the corpus cavernosum, restoring erectile function in diabetic models [38]. Our findings align with these reports, showing that RAG upregulates HMOX1, suppresses hypoxia-induced damage, and restores penile histology and the smooth muscle-to-collagen ratio.

Despite these promising results, several limitations remain. The multicomponent composition of RAG complicates identification of the most critical therapeutic agents. While our network pharmacology analysis highlighted core active compounds, further studies are needed to validate their individual contributions. Additionally, we did not explore MAPK and cAMP signaling pathways in depth, which may play roles in mediating RAG effects. Finally, our study evaluated only short-term outcomes; future research should investigate long-term efficacy and safety to comprehensively assess RAG as a therapeutic strategy for DMED.

Conclusion

This study combined network pharmacology, molecular docking, and in vivo experiments to systematically explore the multi-component, multi-target interactions of RAG in the context of DMED. Our integrated approach offers a holistic perspective on the potential mechanisms of traditional Chinese medicine in managing complex diseases. Bioinformatics analyses identified INS, CAT, BDNF, CASP3, CRP, and HMOX1 as pivotal targets, with hypoxia-related signaling pathways playing a central role in disease progression. Experimental validation in DMED rats confirmed that RAG ameliorated penile tissue damage and modulated the expression of key proteins, including HIF-1α, eNOS, iNOS, and HMOX1, within the hypoxia-responsive pathway. These findings suggest

that RAG can effectively mitigate erectile dysfunction induced by diabetes, providing a promising alternative therapeutic strategy. Nevertheless, additional in vitro and in vivo studies are necessary to further clarify the detailed mechanisms and therapeutic potential of RAG in DMED.

Acknowledgments: None

Conflict of Interest: None

Financial Support: This work was financially supported by the Zhejiang Provincial Natural Science Foundation of China (No.MS25H270044), the Zhejiang Province Traditional Chinese Medicine Inheritance and Innovation Talent Support Program(Nos.2025ZR071), the National Natural Science Foundation of China (Nos. 81804092, 82104855), Young Elite Scientists Sponsorship Program by CACM (No. CACM-2022-QNRC2-A01), the 74th batch of general funding from the China Postdoctoral Science Foundation (No. 2023M743146) and Scientific Research Project Talent Program of Zhejiang Chinese Medical University (No. 2023RCZXZK47).

Ethics Statement: None

References

1. Vita R, Benvenga S, Giammusso B, La Vignera S. Determinants of early response to low-intensity extracorporeal shockwaves for the treatment of vasculogenic erectile dysfunction: an open-label, prospective study. J Clin Med. 2019;8(7):1017–28. doi:10.3390/jcm8071017
2. Defeudis G, Mazzilli R, Tenuta M, Rossini G, Zamponi V, Olana S, et al. Erectile dysfunction and diabetes: a melting pot of circumstances and treatments. Diab Metab Res Rev. 2022;38(2):e3494. doi:10.1002/dmrr.3494
3. Kouidrat Y, Pizzol D, Cosco T, Thompson T, Carnaghi M, Bertoldo A, et al. High prevalence of erectile dysfunction in diabetes: a systematic review and meta-analysis of 145 studies. Diabet Med. 2017;34(9):1185–92. doi:10.1111/dme.13403
4. Malavige LS, Levy JC. Erectile dysfunction in diabetes mellitus. J Sex Med. 2009;6(5):1232–47. doi:10.1111/j.1743-6109.2008.01168.x
5. Shamloul R, Ghanem H. Erectile dysfunction. Lancet. 2013;381(9861):153–65. doi:10.1016/S0140-6736(12)60520-0
6. Ouyang B, Xie Y, Zhang C, Deng C, Lv L, Yao J, et al. Extracellular vesicles from human urine-derived stem cells ameliorate erectile dysfunction in a diabetic rat model by delivering proangiogenic microRNA. Sex Med. 2019;7(2):241–50. doi:10.1016/j.esxm.2019.02.001
7. Maxwell AJ. Mechanisms of dysfunction of the nitric oxide pathway in vascular diseases. Nitric Oxide. 2002;6(2):101–24. doi:10.1006/niox.2001.0394
8. Ryu JK, Suh JK, Burnett AL. Research in pharmacotherapy for erectile dysfunction. Transl Androl Urol. 2017;6(2):207–15. doi:10.21037/tau.2016.11.17
9. Bondeva T, Heinzig J, Ruhe C, Wolf G. Advanced glycated end-products affect HIF-transcriptional activity in renal cells. Mol Endocrinol. 2013;27(11):1918–33. doi:10.1210/me.2013-1036
10. Glancy B, Hartnell LM, Combs CA, Femnou A, Sun J, Murphy E, et al. Power grid protection of the muscle mitochondrial reticulum. Cell Rep. 2018;23(9):2832. doi:10.1016/j.celrep.2018.05.055
11. Ma H, Li Y, Hou T, Li J, Yang L, Guo H, et al. Sevoflurane postconditioning attenuates hypoxia/reoxygenation injury of cardiomyocytes under high glucose by regulating HIF-1α/MIF/AMPK pathway. Front Pharmacol. 2020;11:624809. doi:10.3389/fphar.2020.624809
12. Padmanabhan P, Mccullough AR. Penile oxygen saturation in the flaccid and erect penis in men with and without erectile dysfunction. J Androl. 2007;28(2):223–8. doi:10.2164/jandrol.106.001313
13. Lv B, Zhao J, Yang F, Huang X, Chen G, Yang K, et al. Phenotypic transition of corpus cavernosum smooth muscle cells subjected to hypoxia. Cell Tissue Res. 2014;357(3):823–33. doi:10.1007/s00441-014-1902-0
14. Dwivedi PS, Patil R, Khanal P, Gurav NS, Murade VD, Hase DP, et al. Exploring the therapeutic mechanisms of Cassia glauca in diabetes mellitus through network pharmacology, molecular docking and molecular dynamics. RSC Adv. 2021;11(62):39362–75. doi:10.1039/D1RA07661B

15. Tan YQ, Chen HW, Li J, Wu QJ. Efficacy, Chemical constituents, and pharmacological actions of Radix Paeoniae Rubra and Radix Paeoniae Alba. Front Pharmacol. 2020;11:1054. doi:10.3389/fphar.2020.01054
16. Le N, Zhou X, Fei WT, Liu JL, Liu YB, Zhang JJ, et al. Effects of Radix Paeoniae rubra, Radix Paeoniae Alba, paeoniflorin and albiflorin on hemorheology and vascular endothelial function in rats with acute blood stasis syndrome. Global Tradit Chin Med. 2019;12:1302–7 doi:10.3969/j.issn.1674-1749.2019.09.002
17. Huang CY, Kuo WW, Kuo CH, Tsai FJ, Liu PY, Hsieh DJY. Protective effect of Danggui (Radix Angelicae sinensis) on angiotensin II-induced apoptosis in H9c2 cardiomyoblast cells. BMC Complement Altern Med. 2014;14:358. doi:10.1186/1472-6882-14-358
18. Gong W, Zhu S, Chen C, Yin Q, Li X, Du G, et al. The anti-depression effect of angelicae sinensis radix is related to the pharmacological activity of modulating the hematological anomalies. Front Pharmacol. 2019;10:192. doi:10.3389/fphar.2019.00192
19. Luo Y, Wang Q, Zhang Y. A systems pharmacology approach to decipher the mechanism of danggui-shaoyao-san decoction for the treatment of neurodegenerative diseases. J Ethnopharmacol. 2016;178:66–81. doi:10.1016/j.jep.2015.12.011
20. Guo S, Wang G, Yang Z. Ligustilide alleviates the insulin resistance, lipid accumulation, and pathological injury with elevated phosphorylated AMPK level in rats with diabetes mellitus. J Recept Signal Transduction Res. 2021;41(1):85–92. doi:10.1080/10799893.2020.1789877
21. Hopkins AL. Network pharmacology: the next paradigm in drug discovery. Nat Chem Biol. 2008;4(11):682–90. doi:10.1038/nchembio.118
22. Shah U, Shah R, Acharya S, Acharya N. Novel anticancer agents from plant sources. Chin J Nat Med. 2013;11(1):16–23. doi:10.3724/SP.J.1009.2013.00016
23. Ru J, Li P, Wang J, Zhou W, Li B, Huang C, et al. TCMSP: a database of systems pharmacology for drug discovery from herbal medicines. J Cheminform. 2014;6:13. doi:10.1186/1758-2946-6-13
24. Ma JX, Wang B, Li HS, Yu J, Hu HM, Ding CF, et al. Uncovering the mechanisms of leech and centipede granules in the treatment of diabetes mellitus-induced erectile dysfunction utilising network pharmacology. J Ethnopharmacol. 2021;265:113358. doi:10.1016/j.jep.2020.113358
25. Tzeng TF, Liou SS, Liu IM. The selected traditional Chinese medicinal formulas for treating diabetic nephropathy: perspective of modern science. J Tradit Complement Med. 2013;3(3):152–8. doi:10.4103/2225-4110.114893
26. Xiaobing L, Chunling N, Wenyu C, Yan C, Zhenzhen L. Effect of Danggui-Shaoyao-San-containing serum on the renal tubular epithelial-mesenchymal transition of diabetic nephropathy. Curr Pharm Biotechnol. 2020;21(12):1204–12. doi:10.2174/1389201021666200416094318
27. Loizou S, Lekakis I, Chrousos GP, Moutsatsou P. Beta-sitosterol exhibits anti-inflammatory activity in human aortic endothelial cells. Mol Nutr Food Res. 2010;54(4):551–8. doi:10.1002/mnfr.200900012
28. Bass VL, Soukup JM, Ghio AJ, Madden MC. Oleic acid and derivatives affect human endothelial cell mitochondrial function and vasoactive mediator production. Lipids Health Dis. 2020;19(1):128. doi:10.1186/s12944-020-01296-6
29. Martelli A, Flori L, Gorica E, Piragine E, Saviano A, Annunziata G, et al. Vascular effects of the polyphenolic nutraceutical supplement Taurisolo®: focus on the protection of the endothelial function. Nutrients. 2021;13(5):1540. doi:10.3390/nu13051540
30. Babu S, Krishnan M, Rajagopal P, Periyasamy V, Veeraraghavan V, Govindan R, et al. Beta-sitosterol attenuates insulin resistance in adipose tissue via IRS-1/Akt mediated insulin signaling in high fat diet and sucrose induced type-2 diabetic rats. Eur J Pharmacol. 2020;873:173004. doi:10.1016/j.ejphar.2020.173004
31. Zhang Y, Liang Y, Liu H, Huang Y, Li H, Chen B. Paeoniflorin attenuates gestational diabetes via Akt/mTOR pathway in a rat model. Food Nutr Res. 2020;64:1 doi:10.29219/fnr.v64.4362
32. Cengiz T, Kaya E, Oral DY, Ozakca I, Bayatli N, Karabay AZ, et al. Intracavernous injection of human umbilical cord blood mononuclear cells improves erectile dysfunction in streptozotocin-induced diabetic rats. J Sex Med. 2017;14(1):50–8. doi:10.1016/j.jsxm.2016.11.314
33. Cerychova R, Pavlinkova G. HIF-1, metabolism, and diabetes in the embryonic and adult heart. Front Endocrinol. 2018;9:460. doi:10.3389/fendo.2018.00460
34. Ayer A, Zarjou A, Agarwal A, Stocker R. Heme oxygenases in cardiovascular health and disease. Physiol Rev. 2016;96(4):1449–508. doi:10.1152/physrev.00003.2016

35. He R, Wang Z, Cui M, Liu S, Wu W, Chen M, et al. HIF1A alleviates compression-induced apoptosis of nucleus pulposus derived stem cells via upregulating autophagy. Autophagy. 2021;17(11):3338–60. doi:10.1080/15548627.2021.1872227
36. Dunn LL, Kong SM, Tumanov S, Chen W, Cantley J, Ayer A, et al. Hmox1 (heme oxygenase-1) protects against ischemia-mediated injury via stabilization of HIF-1α (hypoxia-inducible factor-1α). Arterioscler Thromb Vasc Biol. 2021;41(1):317–30. doi:10.1161/ATVBAHA.120.315393
37. Ockaili R, Natarajan R, Salloum F, Fisher BJ, Jones D, Fowler III AA, et al. HIF-1 activation attenuates postischemic myocardial injury: role for heme oxygenase-1 in modulating microvascular chemokine generation. Am J Physiol Heart Circ Physiol. 2005;289(2):H542–8. doi:10.1152/ajpheart.00089.2005
38. Wang Z, Mao Y, Zang Y, Zha Y, Sun J, Wei Z, et al. Transcriptomic analysis reveals the mechanism of isorhamnetin in the treatment of diabetes mellitus erectile dysfunction. Free Radic Biol Med. 2024;224:366–81. doi:10.1016/j.freeradbiomed.2024.08.043